Journal of Materials Chemistry C

Single crystal field-effect transistor of tetrabenzoporphyrin with one-dimensionally extended columnar packing motif exhibiting efficient charge transport property

Journal:	*Journal of Materials Chemistry C*
Manuscript ID	TC-COM-07-2021-003547.R2
Article Type:	Communication
Date Submitted by the Author:	08-Sep-2021

Complete List of Authors:	Zhu, Juanjuan; Nara Institute of Science and Technology Hayashi, Hironobu; Nara Institute of Science and Technology Meng, Chan; Beijing University of Chemical Technology Xiao, Chengyi; Beijing University of Chemical Technology, Matsuo, Kyohei; Nara Institute of Science and Technology Aratani, Naoki; Nara Institute of Science and Technology, Graduate School of Materials Science Zhang, Lei; Beijing University of Chemical Technology Yamada, Hiroko; Nara Institute of Science and Technology, Graduate School of Material Science

COMMUNICATION

Single crystal field-effect transistor of tetrabenzoporphyrin with one-dimensionally extended columnar packing motif exhibiting efficient charge transport property

Received 00th January 20xx,
Accepted 00th January 20xx

DOI: 10.1039/x0xx00000x

Juanjuan Zhu,[a] Hironobu Hayashi,*[a] Meng Chen,[b] Chengyi Xiao,[b] Kyohei Matsuo,[a] Naoki Aratani,[a] Lei Zhang,*[b] and Hiroko Yamada*[a]

5,15-Bis(triisopropylsilyl)ethynyltetrabenzoporphyrin (TIPS-H$_2$BP) gave one-dimensionally extended columnar packing motif. Single crystal field-effect transistor of TIPS-H$_2$BP exhibited clearly better hole mobility (2.16 cm^2 V^{-1} s^{-1}) than its metal complexes (ca. 0.1 cm^2 V^{-1} s^{-1}), with the efficient charge transports through π–π stacking along tetrabenzoporphyrin units.

The charge transport in organic semiconductors is achieved by the π orbital overlapping of the conjugated molecules along the direction of carrier flow. Therefore, organic semiconducting materials with a rigid and planar π-system have a great potential to provide the suitable packing to increase the π orbital overlap.[1–4] Due to the large and rigid π-system, tetrabenzoporphyrins (**BP**s) are promising candidates as efficient p-type semiconducting materials.[5,6] However, **BP** itself is hardly soluble in organic solvents, resulting in the difficulty in its direct solution deposition. In addition, the solubility is an important factor not only for the solution-processable device fabrication but also for achieving the large-scale synthesis by conventional organic chemistry together with easy purification by column chromatography. Although these factors, rigidity and solubility, are likely a trade-off relationship, several molecules perfectly satisfy these requirements. For example, 6,13-bis(triisopropylsilylethynyl)pentacene (**TIPS-Pen**), which is a benchmark compound as an efficient organic semiconducting material, has proven to be quite successful, despite the fact that the pentacene itself is almost insoluble in common organic solvents.[7] Taking advantage of the improved solubility by the introduction of TIPSethynyl groups, the solution sharing with a micropillar-patterned blade gave the hole mobility up to 11 cm^2 V^{-1} s^{-1},[8] achieving clearly better hole mobility than pristine pentacene.

For **BP**s as well, recent synthetic efforts had solved the solubility problem by using “precursor method”, in which a soluble precursor compound, 1,4:8,11:15,18:22,25-tetraethano-29*H*,31*H*-tetrabenzo[*b*,*g*,*l*,*q*]porphyrin (**CP**), can be quantitatively converted to **BP** by a thermally induced retro-Diels-Alder reaction with heating at 150–200 °C for several minutes.[6,9] Importantly, the retro-Diels-Alder reaction releases only ethylene molecules as gaseous byproducts. Thus, no purification process is required to obtain pure compounds, if the corresponding precursors are sufficiently pure. The charge-carrier mobility of **BP** polycrystalline film obtained *via* precursor method was firstly evaluated by Aramaki, exhibiting the hole mobility of 0.017 cm^2 V^{-1} s^{-1}.[10] The hole mobility was then slightly improved to 0.07 cm^2 V^{-1} s^{-1}, while the value was still low.[11] Recently, the substituent effect was evaluated to obtain better charge transport property by controlling the packing orientation of **BP**. It was found that 5,15-bis(triisopropylsilylethynyl)-**BP** (**TIPS-H$_2$BP**) with reasonable solubility for solution-processed organic thin film transistors formed two types of packing motifs: columnar motif by drop-casting and brickwork motif by dip-coating method.[12] The drop-casting films with the columnar motif showed low hole mobility (0.027 cm^2 V^{-1} s^{-1}), although such a columnar motif is also known to exhibit efficient charge transport property. On the other hand, the brickwork motif has two dimensionally extended π-stacking. The maximum hole mobility of dip-coating films reached 1.1 cm^2 V^{-1} s^{-1}, which was approximately 14 times higher than pristine free-base **BP** (0.07 cm^2 V^{-1} s^{-1}). This disparity in charge transport property derived from different packing motif prepared by drop-casting and dip-coating methods turned our attention to single-crystal field-effect transistors (SCFETs), which are able to unveil the intrinsic charge transport property of organic semiconducting materials due to ordered arrangement of molecules, free of grain boundaries and minimized defects. The obtained maximum hole mobility of **TIPS-H$_2$BP** in the above report[12] implied that functionalized **BP**

[a] Division of Materials Science, Nara Institute of Science and Technology (NAIST), 8916-5 Takayama-cho, Ikoma, Nara 630-0192, Japan.
[b] Beijing Advanced Innovation Center for Soft Matter Science and Engineering & State Key Laboratory of Organic-Inorganic Composites, Beijing University of Chemical Technology, Beijing 100029, P. R. China.
† Footnotes relating to the title and/or authors should appear here.
Electronic Supplementary Information (ESI) available: [details of any supplementary information available should be included here]. See DOI: 10.1039/x0xx00000x

derivatives could be candidates for efficient organic semiconducting materials. For further structural fine-tuning of **BP**, the potential of **TIPS-H$_2$BP** as a simple prototype is necessary to be evaluated by using the single crystal.[13–16] In this study, single crystals of **TIPS-H$_2$BP** and its metal complexes were prepared on a substrate, and the molecular orientation in the single crystal was explored in detail. Then, the relationship between the molecular orientation and charge transport property was investigated by preparing SCFETs.

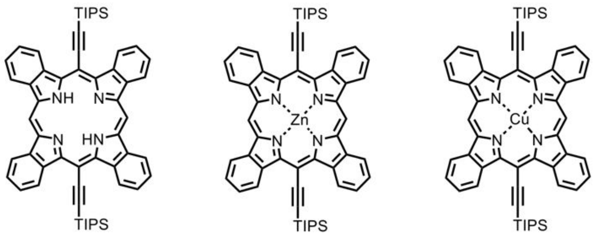

TIPS-H$_2$BP **TIPS-ZnBP** **TIPS-CuBP**

Fig. 1. The structure of **TIPS-H$_2$BP** and its metal complexes employed in this study.

TIPS-H$_2$BP and the zinc(II) and copper(II) complexes (**TIPS-ZnBP** and **TIPS-CuBP**) were synthesized by following the previous reports (Fig. 1).[17] Then, their crystals were grown by drop-casting the toluene solution on octadecyltrichlorosilane (OTS) modified Si/SiO$_2$ surface. It was found that slow evaporation of the drop-casted toluene solution gave isolated and thin ribbon-shaped single crystals on Si/SiO$_2$/OTS substrates (Fig. 2). Importantly, the changing of interfacial color in polarized optical microscope (POM) images indicated that they were single crystals. Narrow ribbon-shaped crystals of **TIPS-H$_2$BP** similar to the case of **TIPS-CuBP** were also observed. However, out-of-plane X-ray diffraction (XRD) and transmission electron microscopy (TEM) analyses indicated that the molecular orientation in these crystals were the same (*vide infra*). Indeed, the crystal was grown as the different shape probably because of the slightly different surface energy on a substrate.[18] Here, the order of ease of crystal formation was as follows: **TIPS-H$_2$BP** > **TIPS-ZnBP** > **TIPS-CuBP**. Specifically, single crystals of **TIPS-CuBP** suitable for SCFETs were hardly obtained on a Si/SiO$_2$/OTS substrate, usually giving a fiber-like structure (Fig. S1).

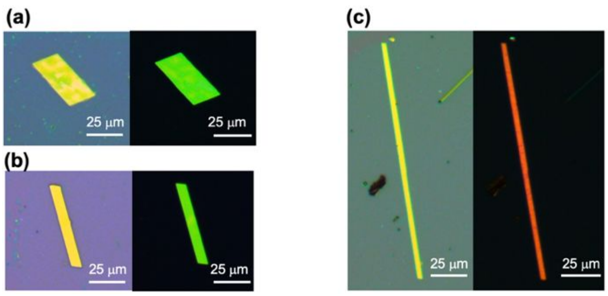

Figure 2. Typical POM images of ribbon-shaped single crystal of (a) **TIPS-H$_2$BP**, (b) **TIPS-ZnBP**, and (c) **TIPS-CuBP** on OTS modified Si/SiO$_2$ substrate. Concentrations for drop-casting of toluene solution: 1.0 mg/ml (**TIPS-H$_2$BP** and **TIPS-CuBP**), 0.5 mg/ml (**TIPS-ZnBP**).

Before examining the molecular orientation of single crystals on a substrate, the bulk single crystal structures for each **BP** derivative were analyzed in order to establish a referential basis for further discussion. Those single crystals were prepared from toluene solutions, although the X-ray analysis had already been done with single crystals obtained from different solvent system in the previous report.[12,17] In fact, solvents showed no significant effect on their packing structures. Briefly, a large **TIPS-H$_2$BP** core (Fig. 3a,b) formed a one-dimensionally extended columnar π-stacking motif with the plane-to-plane distance of **BP** of ca. 3.3 Å (Fig. 3c).[18] **TIPS-H$_2$BP** molecules stacked orthogonally in the packing, alternately possessing planar **TIPS-H$_2$BP** molecule (Fig. 3a) and the one with two TIPSethynyl groups bend from the **BP** plane sigmoidally (Fig. 3b). It is evident that the well-ordered alignment of **TIPS-H$_2$BP** facilitates the intermolecular charge transport in the column. **BP** backbones of **TIPS-ZnBP**[19] and **TIPS-CuBP**[20] are similar to the one of **TIPS-H$_2$BP**. However, molecules in the single crystal form a triad-like structure in which the molecules are stacked orthogonally.[17] In the triad-like structure, **TIPS-ZnBP** and **TIPS-CuBP** also have the plane-to-plane distance of ca. 3.3 Å, while the triad units are packed parallel to provide one-dimensional slip-stacked structures. In addition, a planar **TIPS-ZnBP** or **TIPS-CuBP** molecule is sandwiched by the respective metal complexes with sigmoidally bend TIPSethynyl groups in the triad-like structure. As the result, a long-range molecular orientation is missing in the cases of **TIPS-ZnBP** and **TIPS-CuBP**, in contrast with that observed in **TIPS-H$_2$BP**.

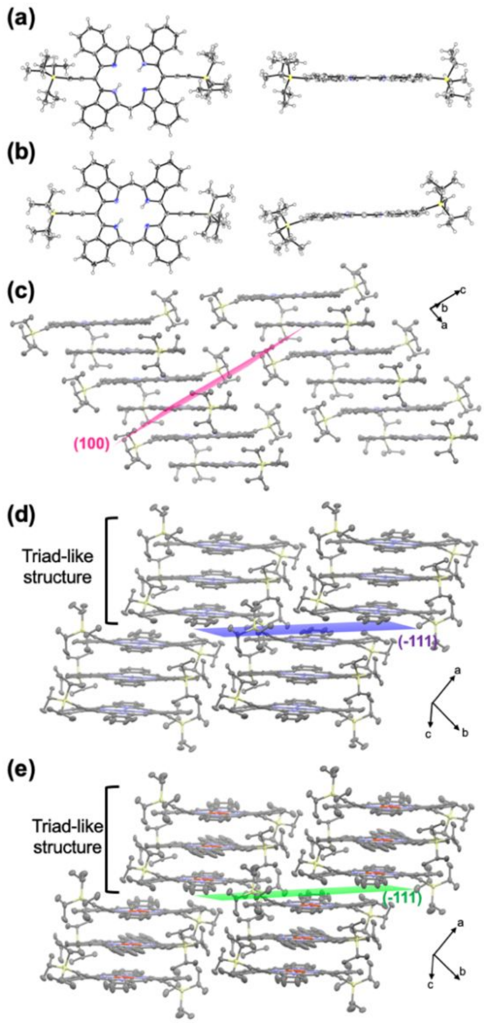

Fig. 3. (a,b) Single crystal X-ray structure of **TIPS-H$_2$BP**. Thermal ellipsoids represent 50% probability. Packing structure of (c) **TIPS-H$_2$BP**, (d) **TIPS-ZnBP**, and (e) **TIPS-CuBP** in the crystals obtained from toluene. Hydrogen atoms are omitted for clarity (c–e).

To shed light on the molecular orientation of single crystals on a substrate, out-of-plane XRD analysis was performed (Fig. 4 and Fig. S2). In the case of **TIPS-H$_2$BP** (Fig. 4a), the intense peaks at 2θ = 5.16° with a *d*-spacing of 17.1 Å together with peaks at 2θ = 6.10° (*d*-spacing = 14.5 Å) and at 2θ = 6.22° (*d*-spacing = 14.2 Å) were well-consistent with the simulated [001], [010], and [011] diffractions of one-dimensional columnar structure (Fig. 3c), respectively, according to the crystallographic data for the bulk crystal. These results support that the one-dimensional columnar packing in parallel to the substrate was grown through π–π stacking direction of **TIPS-H$_2$BP**. Note that a peak at 4.66°, which corresponds to [001] of the brickwork motif,[12] was not observed. Similarly, the peaks at 2θ = 5.02° (*d*-spacing = 17.6 Å) and at 2θ = 5.77° (*d*-spacing = 15.3 Å) for **TIPS-ZnBP** are good agreement with the simulated [001] and [010] diffractions of **TIPS-ZnBP** columnar structure, respectively (Fig. 4b). In the case of **TIPS-CuBP**, small peaks at 2θ = 5.03° (*d*-spacing = 17.6 Å) and at 2θ = 5.82° (*d*-spacing = 15.2 Å) which correspond to [001] and [010], respectively, could be observed (Fig. 4c), while the less amount of single-crystals on the substrate resulted in the overall weak peak intensity of XRD pattern. As described above, fiber-like structure also formed on a substrate together with ribbon-shaped crystals (Fig. S1). Rigid π-systems could form the crystalline nanofibers.[21,22] Thus, these crystalline fibers account for the peaks at 2θ = 4.87° and 2θ = 5.16° which are not consistent with the simulated patterns of the one-dimensional columnar packing.

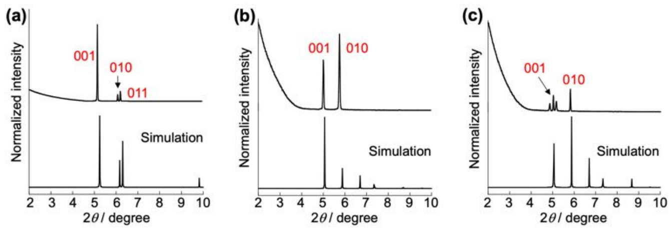

Fig. 4. Experimental out-of-plane XRD and simulated powder XRD patterns of (a) **TIPS-H$_2$BP**, (b) **TIPS-ZnBP**, and (c) **TIPS-CuBP**.

In order to confirm the molecular arrangements in the ribbon-shaped crystals, TEM images and their corresponding selected area electron diffraction (SAED) patterns were collected from an individual ribbon-shaped crystal (Fig. 5). The observed bright diffraction spots demonstrated the high-quality of crystallinity. Here, the SAED pattern could be indexed with its single crystal structure, while the SAED patterns for **TIPS-H$_2$BP** and **TIPS-ZnBP** are not complete. It was found that the preferred crystal growth directions of **TIPS-H$_2$BP**, **TIPS-ZnBP**, and **TIPS-CuBP** were expected to be [100], [–111], and [–111], respectively (Fig. 3c–e), which are in good agreement with the morphologies predicted through the Bravais–Friedel–Donnay–Harker (BFDH)[23–25] method (Fig. 5). Thus, SAED patterns and TEM analysis together with XRD measurement indicated that the growth direction of the ribbon-shaped crystals on the substrate was guided by π–π interactions, creating one-dimensionally extended packing motif as a charge-carrier transport.

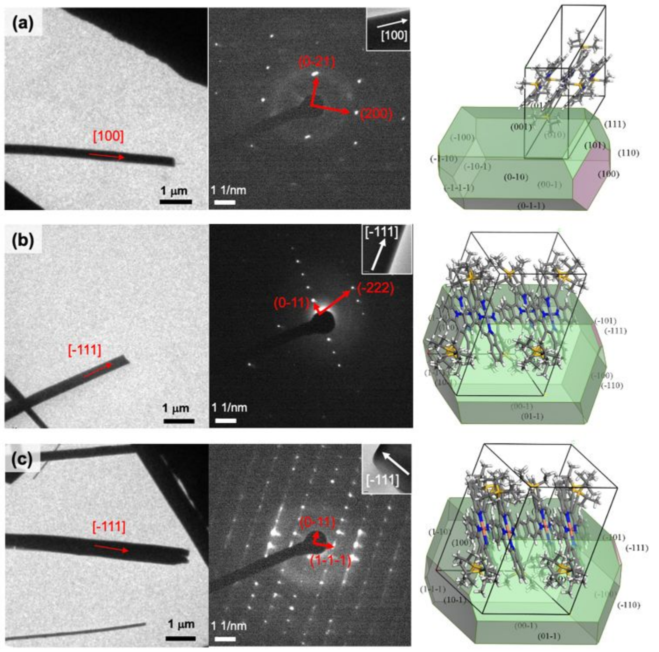

Fig. 5. Representative TEM image, corresponding SAED pattern, and theoretically predicted growth morphology by using the BFDH method of (a) **TIPS-H$_2$BP**, (b) **TIPS-ZnBP**, and (c) **TIPS-CuBP** single crystal.

Finally, the charge transport property of single crystals was evaluated by fabricating bottom-gate-top-contact organic field-effect transistors using "gold layer glue technique".[26] Briefly, gold source and drain electrodes were placed on the crystals which were grown by drop-casting the toluene solution on Si/SiO$_2$/OTS substrate. The effective channel length and width were measured by microscopy (Fig. S3).

The ribbon-shaped crystals of **TIPS-H$_2$BP** exhibited an average value of 1.16 cm^2 V^{-1} s^{-1} with 15 devices (Fig. 6a,d), giving the maximum hole mobility of 2.16 cm^2 V^{-1} s^{-1} with a threshold voltage V_{th} of 15.6 V and on/off ratio I_{on}/I_{off} of 6.1 x 10^2 (Fig. S4). In the previous report, the one-dimensional columnar structure of **TIPS-H$_2$BP** prepared by drop-casting method exhibited the hole mobility of 0.027 cm^2 V^{-1} s^{-1}.[6] Thus, the maximum hole mobility obtained in this study is approximately 87 times higher than that of the drop-casting one. This result supported that the molecular orientation of **TIPS-H$_2$BP** is preferable to SCFETs, with the charge transport through π–π stacking of **BP** units in the one-dimensional column. In addition, the efficient charge transport reflected the feature of single crystals with free of grain boundaries and minimized defects. It should be noted that nearly identical curves were observed after 10 cycles (Fig. S5), suggesting the good bias-stress stability of SCFETs based on ribbon-shaped crystals of **TIPS-H$_2$BP**. Here, SCFET devices based on **TIPS-H$_2$BP** often showed the hole carried on operation mode specially for the device which exhibited the high hole mobility (Fig. S4), indicating that the transport channel already formed even without gate bias (V_G = 0 V). This is probably due to the high hole density of **TIPS-H$_2$BP**. The holes not only filled the trap states, but also the excess holes became free carriers, forming a conducting channel even though at V_G = 0 V. Moreover, the decreased trap states would facilitate carrier transport, thus improved the mobility of **TIPS-H$_2$BP**.[27]

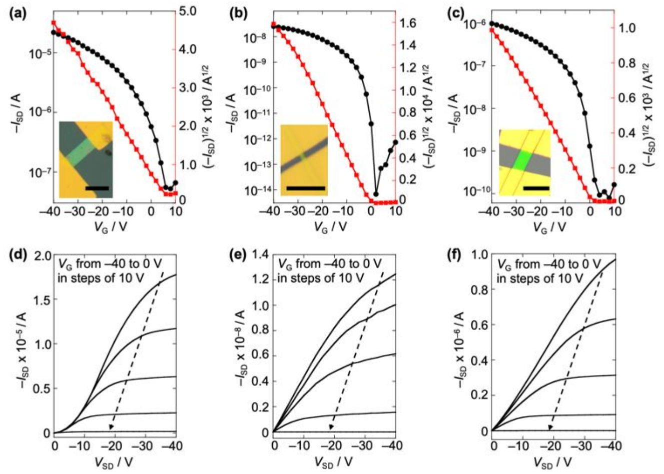

Fig. 6. Typical transfer (a–c) and output (d–f) characteristics of the device of (a, d) **TIPS-H$_2$BP**, (b, e) **TIPS-ZnBP**, and (c, f) **TIPS-CuBP** crystals at a fixed source/drain voltage, V_{SD} = –40 V. Insets show image of device. Scale bar: 25 μm.

On the other hand, the ribbon-shaped crystals of the metal complexes, **TIPS-ZnBP** and **TIPS-CuBP**, showed clearly lower hole mobilities compared with **TIPS-H$_2$BP** (Fig. 6b,c,e,f, and S4), although those values were much higher than the ones prepared by spin-coating method (1.1 x 10^{-5} cm^2 V^{-1} s^{-1} for **TIPS-ZnBP** and 5.6 x 10^{-3} cm^2 V^{-1} s^{-1} for **TIPS-CuBP**).[17] The maximum hole mobility of 0.12 cm^2 V^{-1} s^{-1} (average values of 0.05 cm^2 V^{-1} s^{-1} with 12 devices) with a threshold voltage V_{th} of 6.6 V and on/off ratio I_{on}/I_{off} of 7.6 x 10^5 for **TIPS-ZnBP**, while **TIPS-CuBP** showed the maximum hole mobility of 0.16 cm^2 V^{-1} s^{-1} (average values of 0.14 cm^2 V^{-1} s^{-1} with 4 devices) with a threshold voltage V_{th} of 3.0 V and on/off ratio I_{on}/I_{off} of 1.1 x 10^3. This result is rationalized by the fact that charge transport is suppressed in the cases of **TIPS-ZnBP** and **TIPS-CuBP** because of their triad-like structures (Fig. 3), clearly indicating the metalation had negative effects on the charge transport property.

Note that the *I-V* characteristics for **TIPS-ZnBP** device seem suppressed at high gate voltage, and the linear portion of the **TIPS-H$_2$BP** device shows current crowding. Although these reasons are not clear at this moment as the mechanisms are very complex, the carrier-density-dependent mobility and contact resistance are known to be two important factors which cause nonideal characteristics.[28–31] Here, the gate-dependence saturation mobility extracted from *I-V* curves is shown in Fig S6. Most OFET devices of **TIPS-H$_2$BP** showed the mobility with gate voltage independency (Fig. S6a). However, a few devices exhibited decreased mobility with increased gate voltage (Fig. S6c), which may be attributed to the charge trapping induced non-ideal behaviors.[32] Distinctly, the *I-V* characteristics for all the **TIPS-ZnBP** devices showed a typical "double-slope" shape or "kink" with the mobilities shaking upwards and downwards (Fig. S6b and S6d) at different gate voltages[28]. Regarding the single-crystal nature of our devices, these "double-slope" phenomenon may be caused by the disorder of the interface, which means that charges are more tightly attracted toward the interface at high gate voltages.[33,34] Since the nonideality could affect the calculation for the mobility, further analysis will be done to unveil the reason for the nonideality. This effort should contribute to provide an important clue to improving the mobility of **BP** derivatives.

In summary, SCFETs of **TIPS-H$_2$BP** and its metal complexes were fabricated and their charge transport properties were evaluated. **TIPS-H$_2$BP** exhibited the best mobility (2.16 cm^2 V^{-1} s^{-1}) among the **BP** derivatives employed in this study. XRD and TEM analyses unveiled that the long-range one-dimensional columnar structure of **TIPS-H$_2$BP** contributed the high charge transport property. It should be noted that the deviation between the maximum and average hole mobilities of **TIPS-H$_2$BP** would stem from the quality of single crystals, meaning that finding of optimized conditions for single crystal formation could improve the charge transport property. More importantly, recent synthetic efforts are providing the variety of **BP** derivatives.[6,35–37] Considering that **TIPS-H$_2$BP** shows excellent stability, elaborately-designed **BP** derivatives have a great potential to be promising semiconducting materials. We believe that fine-tuning of **BP** structure enables the significant improvement in the charge transport property.

Conflicts of interest

There are no conflicts to declare.

Acknowledgements

This work was partly supported by CREST JST (No. JPMJCR15F1) and Grants-in-Aid for Scientific Research (Nos. JP20H02816, JP20H00379, JP20H05833, JP20H02711, JP20K15261). We thank Shohei Katao (NAIST) for XRD and X-ray single crystal analyses, and Sakiko Fujita and Tomoko Ohno (NAIST) for TEM measurement, respectively.

Notes and references

1 V. Coropceanu, J. Cornil, D. A. S. Filho, Y. Olivier, R. Silbey, and J Brédas, *Chem. Rev.*, 2007, **107**, 926–952.
2 B. Kuei, and E. D. Gomez, *Soft Matter*, 2017, **13**, 49–67.
3 C. Zhan, and J. Yao, *Chem. Mater.*, 2016, **28**, 1948–1964.
4 J. Mei, Y. Diao, A. L. Appleton, L. Fang, and Z. Bao, *J. Am. Chem. Soc.*, 2013, **135**, 6724–6746.
5 C. M. B. Carvalho, T. J. Brocksom, and K. T. Oliveira, *Chem. Soc. Rev.*, 2013, **42**, 3302–3317.
6 H. Yamada, D. Kuzuhara, M. Suzuki, H. Hayashi, and N. Aratani, *Bull. Chem. Soc. Jpn.*, 2020, **93**, 1234–1267.
7 J. E. Anthony, J. S. Brooks, D. L. Eaton, and S. R. Parkin, *J. Am. Chem. Soc.*, 2001, **123**, 9482–9483.
8 Y. Diao, B. C.-K. Tee, G. Giri, J. Xu, D. H. Kim, H. A. Becerril, R. M. Stoltenberg, T. H. Lee, G. Xue, S. C. B. Mannsfeld, and Z. Bao, *Nat. Mater.*, 2013, **12**, 665–671.
9 S. Ito, T. Murashima, H. Uno, N. and Ono, *Chem. Commun.*, 1998, 1661–1662.

10 S. Aramaki, Y. Sakai, and N. Ono, *Appl. Phys. Lett.,* 2004, **84**, 2085–6563.
11 N. Noguchi, S. Junwei, H. Asatani, and M. Matsuoka, *Cryst. Growth Des.*, 2010, **10**, 1848–1853.
12 K. Takahashi, B. Shan, X. Xu, S. Yang, T. Koganezawa, D. Kuzuhara, N. Aratani, M. Suzuki, Q. Miao, and H. Yamada, *ACS Appl. Mater. Interfaces*, 2017, **9**, 8211–8218.
13 X. Zhang, H. Dong, and W. Hu, *Adv. Mater.*, 2018, **30**, 1801048.
14 P. Wang, D. Liu, Y. Wang, P. Zhang, P. Yu, M. Wang, Y. Zhen, H. Dong, and W. Hu, *Chin. Chem. Lett.*, 2020, **31**, 2909–2912.
15 F. Yang, L. Sun, Q, Duan, H. Dong, Z. Jing, Y. Yang, R. Li, X. Zhang, W. Hu, and L. Chua, *SmartMat.*, 2021, **2**, 99–108.
16 Z. Qin, H. Gao, H. Dong, and W. Hu, *Adv. Mater.*, 2021, **33**, 2007149.
17 K. Takahashi, N. Yamada, D. Kumagai, D. Kuzuhara, M. Suzuki, Y. Yamaguchi, N. Aratani, K. Nakayama, and H. Yamada, *J. Porphyrins Phthalocyanines.*, 2015, **19**, 465–478.
18 Crystallographic data for **TIPS-H$_2$BP**: $C_{58}H_{62}N_4Si_2$, M_W = 871.29, Triclinic, space group *P*-1, a = 8.9318(8), b = 15.8384(14), c = 18.7438(17) Å, α = 63.316(5)°, β = 78.745(6)°, γ = 81.031(6)°, V = 2354.7 Å^3, T = 103 K, Z = 2, reflections measured 32403, 8610 unique. The final R_1 was 0.0986 ($I > 2\sigma(I)$), and the final wR on F^2 was 0.2446 (all data), GOF = 0.998. CCDC:2099221.
19 Crystallographic data for **TIPS-ZnBP**: $C_{58}H_{60}N_4Si_2Zn$, M_W = 934.65, Triclinic, space group *P*-1, a = 12.9207(2), b = 15.7074(3), c = 19.0205(4) Å, α = 101.5873(7)°, β = 108.2265(7)°, γ = 97.6339(7)°, V = 3511.50 Å^3, T = 103 K, Z = 3, reflections measured 61191, 16079 unique. The final R_1 was 0.0403 ($I > 2\sigma(I)$), and the final wR on F^2 was 0.1127 (all data), GOF = 1.072. CCDC:2099222.
20 Crystallographic data for **TIPS-CuBP**: $C_{58}H_{60}N_4Si_2Cu$, M_W = 932.82, Triclinic, space group *P*-1, a = 12.9584(3), b = 15.6807(3), c = 19.0596(4) Å, α = 101.5277(7)°, β = 108.3473(7)°, γ = 97.3928(7)°, V = 3524.59 Å^3, T = 103 K, Z = 3, reflections measured 60254, 16310 unique. The final R_1 was 0.0621 ($I > 2\sigma(I)$), and the final wR on F^2 was 0.1956 (all data), GOF = 1.156. CCDC:2099223.
21 S. Tanaka, M. Shirakawa, K. Kaneko, M. Takeuchi, and S. Seiji, *Langmuir,* 2005, **21**, 2163–2172.
22 H. Hayashi, N. Aratani, and H. Yamada, *Chem. Eur. J.,* 2017, **23**, 7000–7008.
23 J. D. H. Donnay, and D. Harker, *Am. Mineral.,* 1937, **22**, 446–467.
24 A. L. Briseno, S. C. B. Mannsfeld, X. Lu, Y. Xiong, S. A. Jenekhe, Z. Bao, and Y. Xia, *Nano Lett.,* 2007, **7**, 668–675.
25 C. Wang, Z. Liang, Y. Liu, X. Wang, N. Zhao, Q. Miao, W. Hu, and J. Xu, *J. Mater. Chem.,* 2011, **21**, 15201–15204.
26 L. Jiang, H. Dong, and W. Hu, *J. Mater. Chem.*, 2010, **20**, 4994–5007.
27 H. Wang, X. Wang, H. Huang, and D. Yan, *Appl. Phys. Lett.*, 2008, **93**, 103307.
28 H. Phan, M. J. Ford, A. T. Lill, M. Wang, G. C. Baran, and T.-Q. Nguyen, *Adv. Funct. Mater.*, 2018, **28**, 1707221.
29 T. Uemura, C. Rolin, T.-H. Ke, P. Fesenko, J. Genoe, P. Heremans, and J. Takeya, *Adv. Mater.* 2016, **28**, 151–155.
30 E. G. Bittle, J. I. Basham, T. N. Jackson, O. D. Jurchescu, and D. J. Gundlach, *Nat. Commun.*, 2016, **7**, 10908.
31 M. Waldrip, O. D. Jurchescu, D. J. Gundlach, and E. G. Bittle, *Adv. Funct. Mater.* 2020, **30**, 1904576.
32 H.-L. Un, P. Cheng, T. Lei, C.-Y. Yang, J.-Y. Wang, and J. Pei, *Adv. Mater.*, 2018, **30**, 1800017.
33 J. Takeya, M. Yamagishi, Y. Tominari, R. Hirahara, Y. Nakazawa, T. Nishikawa, T. Kawase, T. Shimoda, and S. Ogawa, *Appl. Phys. Lett.*, 2007, **90**, 102120.
34 H. Sirringhaus, *Adv. Mater.*, 2014, **26**, 1319–1335.
35 S. Kumar, X. Jiang, W. Shan, R. G. W. Jinadasa, K. M. Kadish, H. Wang, *Chem. Commun.*, 2018, **54**, 5303–5306.
36 M. Ruppel, L.-P. Gazetas, D. Lungerich, F. Hamppel, N. Jux, *J. Org. Chem.*, 2020, **85**, 7781–7792.
37 K. Muramatsu, T. Okujima, S. Mori, M. Takase, and H. Uno, *Chem. Lett.*, 2021, **50**, 841–843.